



Contents lists available at ScienceDirect

Engineering Failure Analysis

journal homepage: www.elsevier.com/locate/efa



Understanding the “blue spot”

Sodium chloride hot salt stress-corrosion cracking in titanium-6246 during fatigue testing at low pressure



E.A. Saunders ^{a,*}, T.P. Chapman ^b, A.R.M. Walker ^c, T.C. Lindley ^b, R.J. Chater ^b, V.A. Vorontsov ^b, D. Rugg ^c, D. Dye ^b

^a Rolls-Royce plc, Materials — Failure Investigation, Bristol BS34 7QE, UK

^b Department of Materials, Royal School of Mines, Imperial College London, Prince Consort Road, London SW7 2BP, UK

^c Rolls-Royce plc, Materials, Elton Road, Derby DE24 8BJ, UK

ARTICLE INFO

Article history:

Received 22 April 2015

Accepted 16 June 2015

Available online 23 June 2015

Keywords:

Hot salt stress-corrosion cracking

Titanium-6246

Fractography

Pressure implication

Novel technology application in failure analysis

ABSTRACT

During hot component fatigue tests there have been two cases of low life crack initiation of gas turbine rotating parts manufactured from the Titanium alloy Ti-6246. Both exhibited a small (~0.1 mm) elliptical ‘blue spot’ at the origin. Through validated striation count work and fracture mechanics it was established that fatigue had propagated with a near-nil initiation life. Early investigation suggested that the ‘blue spot’ was possibly a region of stage 1 fatigue growth, and was therefore a material behaviour concern with potential implications for service. During an investigation of a later cracking incident in this alloy, subsequently shown to have resulted from stress-corrosion cracking (SCC), near-identical fractographic characteristics to that seen in the ‘blue spot’ were found that subtly differentiated it from stage 1 fatigue. Also, similar ‘blue spots’ have since been identified on Ti6246 Laboratory hot LCF test specimens and found to have been due to contamination by NaCl, through the application of focussed long-term EDX examination and other novel chemical analyses techniques. By the application of those techniques, fractography, and comparison against these specimens, Rolls-Royce and Imperial College London have collaborated to show that the original two component ‘blue spots’ were subtle examples of NaCl-related Hot Salt Stress-Corrosion Cracking (HSSCC). Such cracking has not been found to occur in service components, due to air pressure within the engine, and the effect is therefore confined to Laboratory and component tests at near-atmospheric pressure or below.

© 2015 Rolls-Royce plc. Published by Elsevier Ltd. All rights reserved.

1. Introduction

Titanium and its alloys spontaneously form stable and continuous surface TiO_2 oxide films on exposure to oxygen – the “passive layer” – the reason for very good protection against corrosive attack [1–3]. Even when the passive layer is broken it instantaneously heals, so long as oxygen is not prevented from reaching it [2].

In addition to this corrosion resistance, high fatigue strength to density ratios [1,3,4] have ensured that titanium alloys have broad applications in aero-gas turbine engines [5,6].

In the gas turbine, due to these properties, there is a desire to use titanium as far back in the engine and at as high a temperature as possible [5], promoting increased strength, higher temperature-resistant alloy development [5,7]. One such is the lamellar-microstructure beta (β)-forged and alpha (α)- β solution heat treated α/β titanium alloy Ti-6Al-2Sn-4Zr-6Mo (Ti-6246) [3,5,8,9], which is found in many components such as compressor discs.

* Corresponding author.

Spin testing of such rotating parts is a fundamental requirement as part of the demonstration of component fatigue life [10].

Two such hot (350, 400 °C) cyclic fatigue spin tests were carried out on Ti-6246 components, and found cracked in low cycle fatigue (LCF) at unexpectedly short lives. For this article only, the two tests have been labelled as ST1 and ST2.

Initial macroscopic fractographic examination at Rolls-Royce revealed tiny optically blue-coloured elliptical features of ~0.1 mm dimension present at the origin of both component crack systems. These have come to be known as the “blue spot” (sometimes “blue/grey”) [11]; Fig. 1.

The “blue spots” were bounded by an abrupt colour change that is unconventional compared to normal ‘growth-out’ temper-colouration on hot cyclic fatigue fracture surfaces [12,13].

Quantitative fractography and fracture mechanics had together indicated that propagation from the “blue spot” periphery had occurred with near-nil initiation life, whilst the initial flaw size calculated via fracture mechanics [14] approximated to the “blue spot” dimension. Thus, it was considered that there was a Ti-6246 material behaviour concern with potential implications for service.

Initial investigation deemed that fractographic characteristics within the blue spot resembled microstructure (“structure-sensitive”; Fig. 2) [15,16]. A stress-corrosion mechanism was considered, but at the time no corrosive species were identified using the available techniques on either ST1 or ST2. It was generally commented that the crack was due to low cycle fatigue (LCF) development, but, although describing the fractographic characteristics within the “blue spot”, no conclusion could be given as to its nature or cause at that time.

A collaborative PhD project was set-up between Rolls-Royce plc (Materials) and Imperial College London, which partly aimed to further understand the ‘blue spot’ crack initiation mechanism [11]. A number of the concepts presented herein have formerly been aired in [11], whilst this article explores other specimen and spinning rig results and related issues – as presented orally in the Sixth International Conference on Engineering Failure Analysis on 9th July 2014 (Lisbon, Portugal).

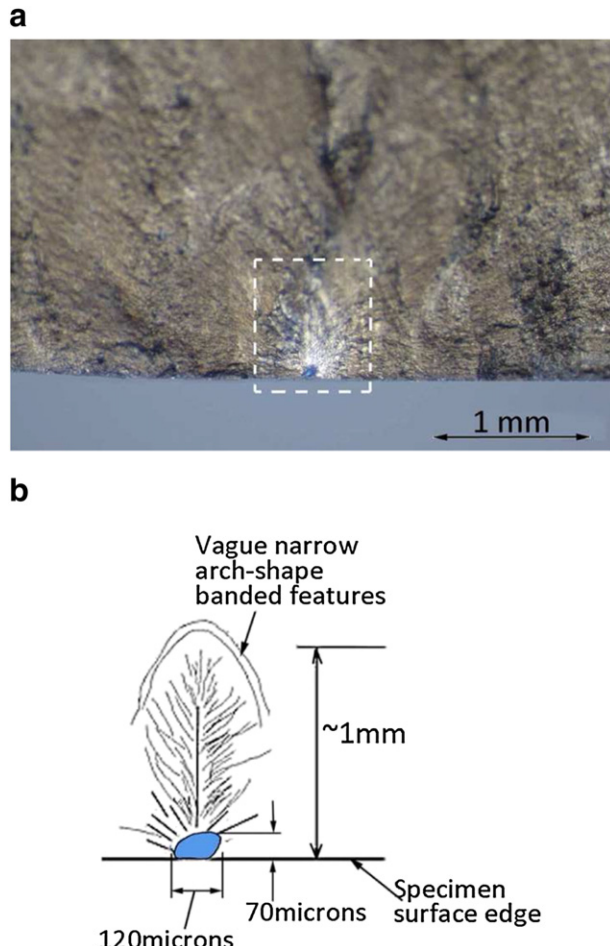


Fig. 1. (a) A ‘blue spot’ may be seen in this optical image of the ST1 crack origin on the fracture surface, located where an aligned alpha lath colony met the surface shown by the fern-shaped region of growth. Such microstructural features are not uncommon in this material (others may be seen in the image, without ‘blue spots’). (b) Schematic of the area highlighted in (a). “Blue spots” in other specimens (including ST2) were not located at aligned alpha lath colonies or other particular microstructural feature.

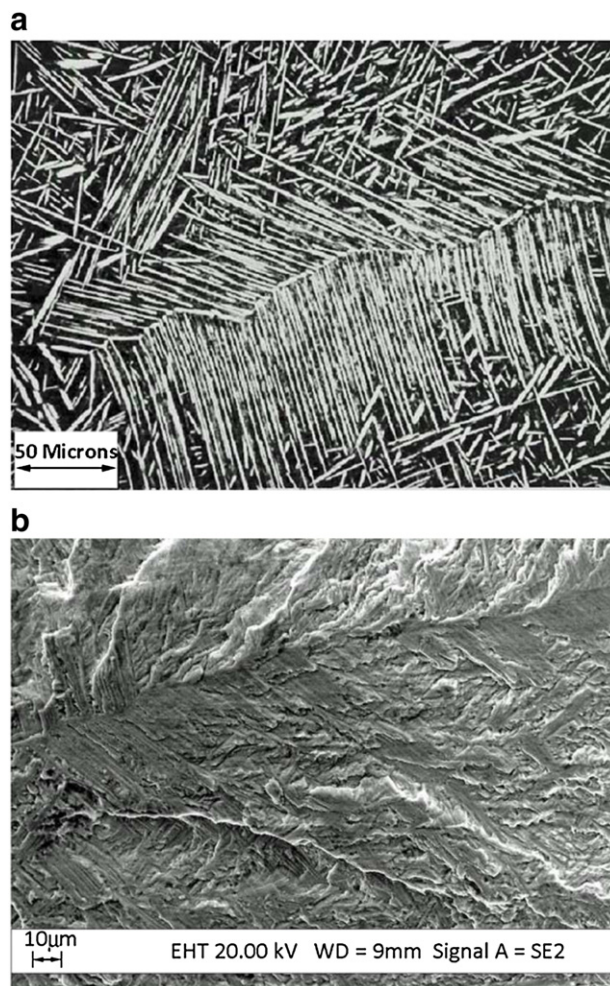


Fig. 2. (a) Optical micrograph of typical microstructure of Ti-6246 (in this case an aligned α colony at a prior β grain boundary can be seen), and (b) a secondary electron image of “structure-sensitive” growth.

2. Fractography

Fractographic examination was carried out on a Leica DMLM Optical Microscope, and a Leo 1550 field emission gun scanning electron microscope (FEG-SEM) located in Rolls-Royce, Bristol.

2.1. Quantitative fractography and “near-nil initiation life”

Quantitative fractography via striation counting methodology [14,17–19] carried out across the main LCF portion of both cracks established ‘blue spot’ formation to have occurred early in the test, and fatigue had developed from it soon after (“near-nil initiation life”).

The validity of measured striation spacings with respect to macroscopic growth rate (da/dN) was confirmed by comparative counting on a corner-crack Ti-6246 LCF specimen with a known test parameters and macroscopic growth rate (via potential-

Table 1

LCF test parameters of samples referred to in this article; test temperature (T), maximum stress amplitude (σ_{\max}), number of cycles to failure (N_f) and R ratio ($\sigma_{\min}/\sigma_{\max}$). All were tested at atmospheric pressure. Specimen ‘LCF133’ was supplied by Rolls-Royce Derby (Elton Road), and ‘LF014’ by Rolls-Royce Deutschland.

Label	T	σ_{\max}	N_f	R	Form	Environment
“LCF133”	450 °C	560 MPa	4474 cycles broken	0	LCF (cylindrical form)	Deliberately NaCl-contaminated
“LF014”	450 °C	600 MPa	9757 cycles broken	0.1	LCF (bowtie form)	Intended as clean. Pressure, atmospheric
“LCF127”	450 °C	640 MPa	50882 cycles broken	0	LCF (cylindrical form)	Datum – not salt-contaminated.

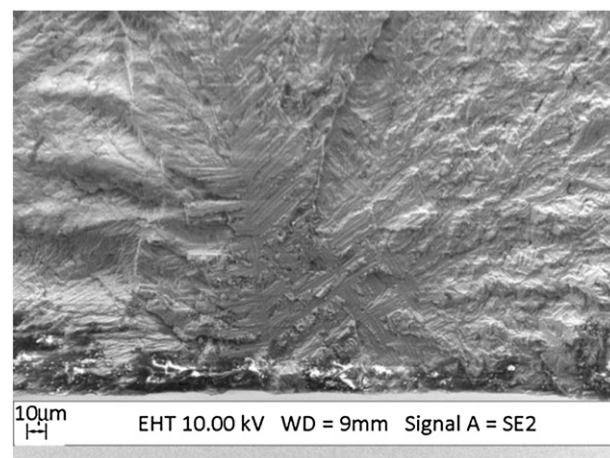


Fig. 3. Secondary electron image showing the “brittle structure-sensitive/trans-lamellar cleavage” fracture appearance of the ST1 origin “blue spot” region.

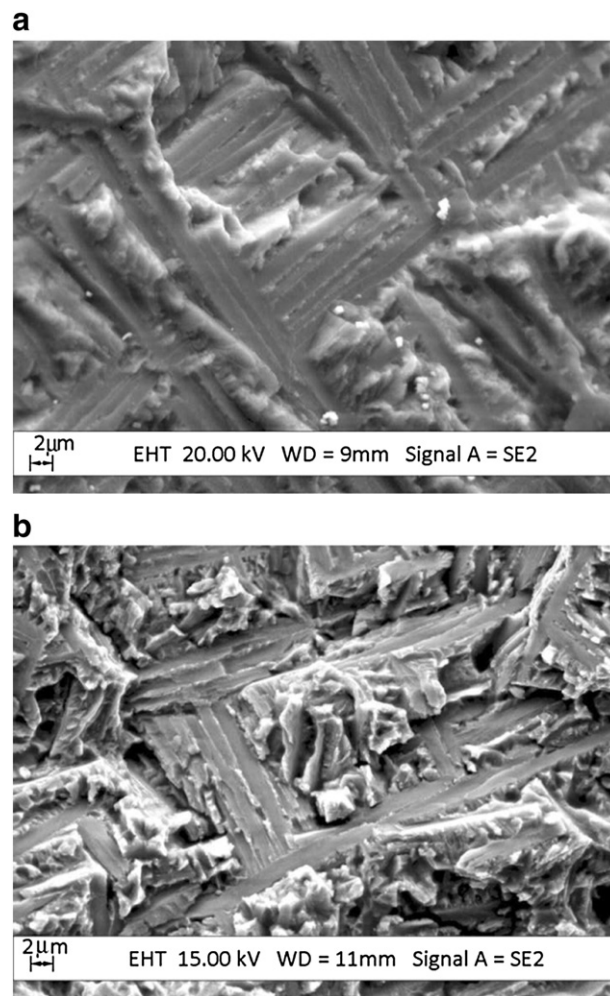


Fig. 4. Secondary electron images of the “brittle structure-sensitive” or “trans-lamellar cleavage” appearance in (a) the ST1 origin “blue spot” region, and (b) a known stress-corrosion crack in Ti-6246 at the same magnification (on that occasion associated with silver chloride, and occurred after the initial investigation work on ST1 and ST2).

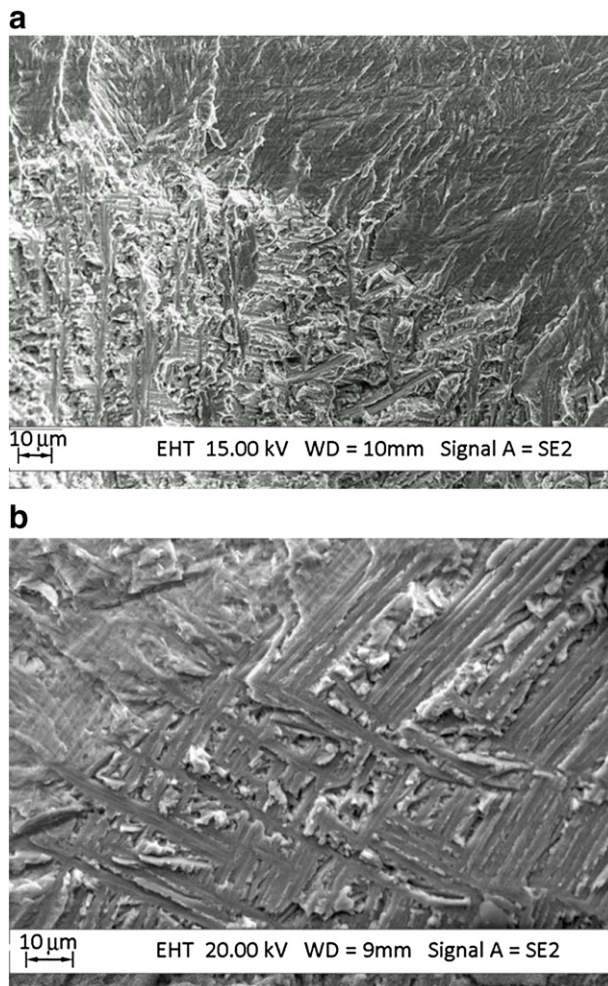


Fig. 5. Transition between “trans-lamellar cleavage” and stage 1 fatigue seen in the same field of view – highlighting the difference in fractography type: (a) from the other ‘known SCC in Ti-6246’ in Fig. 4 – “trans-lamellar cleavage” lower left, and fatigue upper right. (b) From specimen LCF133 – the more brittle “trans-lamellar cleavage” over the majority of the image transitions to a ‘softer’-appearing structure-sensitive fatigue in the upper left corner.

difference monitoring). Striation counting is only valid above a certain value of stress-intensity range, (ΔK) [20,21], that being where an approximate 1:1 ratio of striation to applied load cycle is sufficiently accurate for counting to be useful within its usual bounds of error. That ‘valid’ ΔK (above which striation counting matches actual cycles) is dependent on material and test parameters (stress

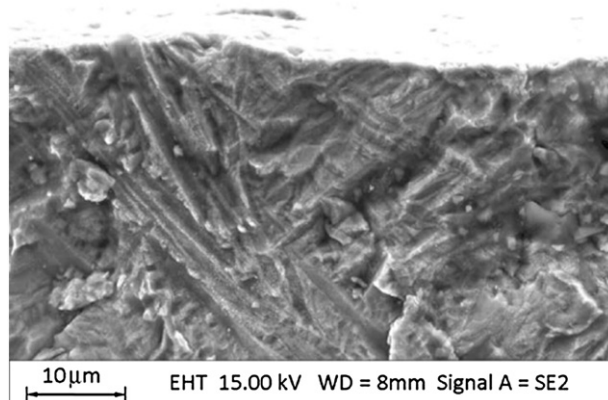


Fig. 6. Secondary electron image of fracture appearance within the test ST2 “blue spot”. The “trans-lamellar cleavage” appearance in this case has less clarity than was observed in ST1 (refer to Fig. 4).

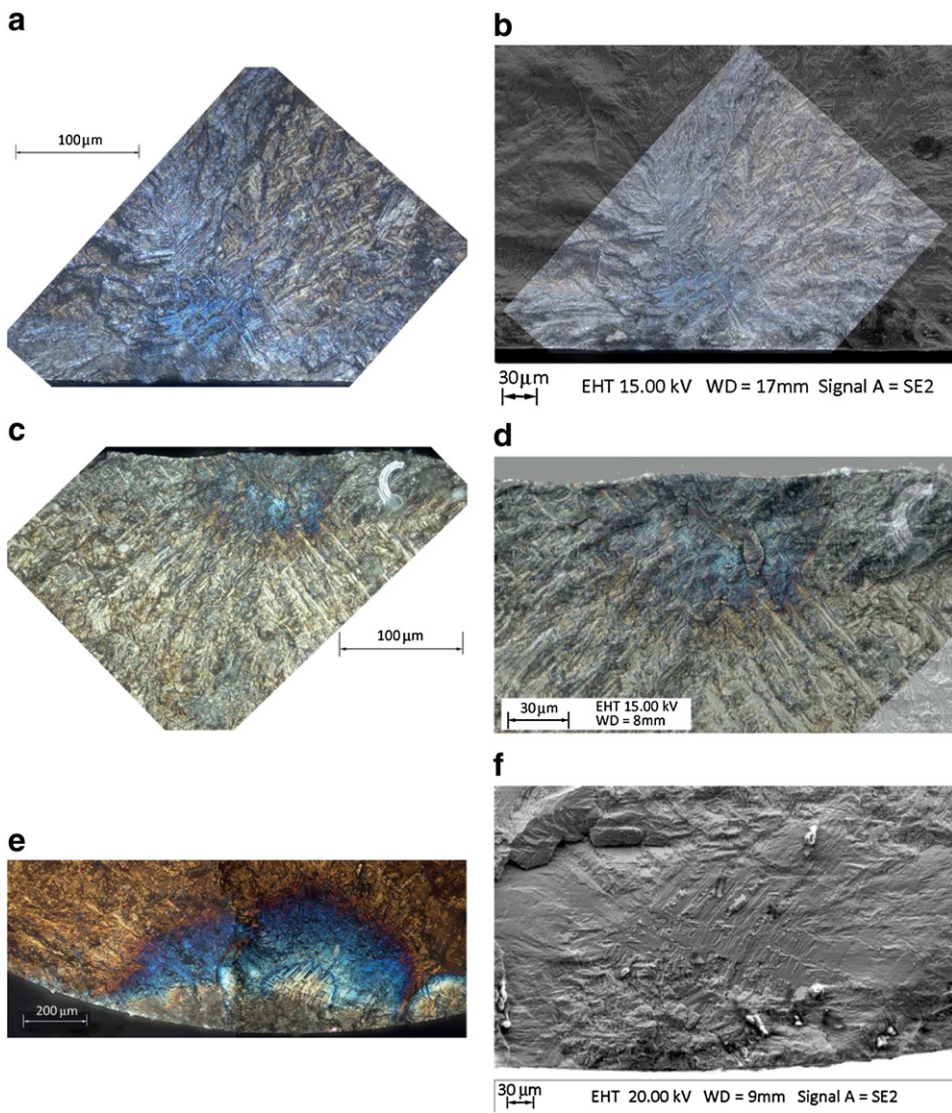


Fig. 7. (a), (b) ST1 and (c), (d) ST2 fractography with optical images and superposed secondary electron images. In ST1, the blue spot was co-located at an aligned alpha-colony aspect, but this was not an aspect of the others shown here. (e), (f) Specimen LCF133. The actual “blue spot” occurs within a region of normal hot LCF growth-out temper colouration, with “trans-lamellar cleavage” visible both optically and in electron optics.

range, R-ratio, temperature), and accordingly was established on the Ti-6246 corner crack specimen above. For both striation counts (on the ST1 and ST2 cracks), the corresponding ΔK values for all striation spacing measurements made above the “Engineering Crack Size” [22] of 0.76 mm (0.030 in.) surface length, were above that value of ΔK in the valid range. Striation counts then indicated very early development of the ‘blue spot’ and transition to fatigue.

Supporting this, a good match of striation count data for ST1 and ST2 was found on comparison with a crack depth (a) versus accumulated cycles (N) curve (“aN-curve”) separately generated via fracture mechanics [23]. Back calculation on the aN-curves from the total number of applied cycles indicated initial flaw sizes (EIFS) of ~0.1 mm, which approximately corresponded to the “blue spot” dimensions, thus further supporting the conclusion of near-nil initiation life in both tests.

A Laboratory hot LCF specimen in Ti6246 “LF014” (Table 1) exhibited “blue spots” that transitioned in the same way from HSSCC to fatigue propagation. Striation counting and fracture mechanics applied in a similar way again found that propagation had occurred with a near-nil initiation life from the periphery of the ‘blue spot’.

2.2. “Blue spot” fractography

Aside from ST1 and ST2, “blue spot” fractography was examined on numerous hot LCF test specimens – some known salt-contaminated, others not. Three of these specimens are referred to in this article (including one datum); Table 1. The ST1 and ST2

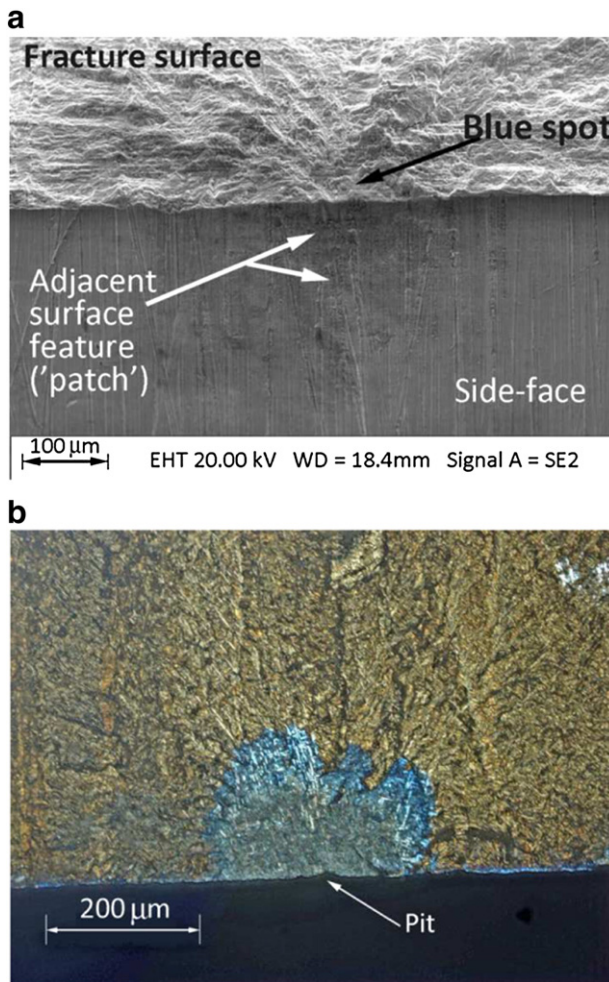


Fig. 8. (a) Example of a specimen side-face 'patch' adjacent to a fracture surface "blue spot" – specimen LF014 tilted to show both the fracture surface (including the blue spot) and side-face. (b) Optical view of the LF014 'blue spot' on the fracture surface, which appears blue-grey centrally with a pit.

test parameters have not been related due to confidentiality reasons, though they were tested at 350 °C and 400 °C at low pressure (2 mbar).

The 'blue spots' exhibited a strongly "structure-sensitive" fractographic appearance, with primary α laths displaying a brittle/cleaved appearance; Figs. 3, 4a (in some cases, separation at primary α lath boundaries to transformed β might have occurred). Secondary α also appeared cleaved, whilst fracture through transformed β had a more ductile nature. This gave rise to a "brittle structure-sensitive" descriptive, though the cleaved nature of the primary α laths may be considered as "trans-lamellar cleavage" alluded to previously [24–26]. For further examples and description refer to [11].

This brittle fractographic appearance has formerly been linked to hot-salt stress corrosion cracking in titanium alloys [11,24–26]. Very similar-appearing fractography had been observed by the authors on a known case of stress-corrosion cracking that had occurred later to the ST1 and ST2 tests, which provided recognition through comparison; Fig. 4b.

On occasion, a nodular oxidation/corrosion product was visible on the surface, obscuring underlying fractography – indicative of an environmentally-assisted crack nucleation system [11].

The appearance of the "trans-lamellar cleavage" fracture mode only *subtly differs* from that of "structure-sensitive" stage 1 fatigue propagation, so recognition of the fracture type was enhanced by viewing transitions from "trans-lamellar cleavage" to fatigue within the same field of view; Fig. 5.

There was variation in the clarity of the "trans-lamellar cleavage", which is proposed to be in part related to the microstructure at the location of fracture (the scale of the primary α lath dimensions and the quantity of transformed β), and also in part related to the level of corrodant initially present and the extent of its reaction (being temperature-dependent). This makes recognition more difficult in some cases – as was found within the ST2 blue spot; Fig. 6.

Optical (microscopic) multi-focus fractographic imagery on the blue spot origins ($200\times$, $500\times$), established a link between the blue colouration and the “brittle structure-sensitive” characteristics observed with electron optics; Fig. 7. The demarcation between the two fractographic types (“trans-lamellar cleavage” to fatigue) was also visible as the blue colouration periphery seen optically.

Certain test specimens exhibited macroscopically visible ‘patches’ of deposit/residue on the side-face immediately adjacent to the blue spot fracture surface; Fig. 8. These patches were often semi-elliptical in appearance (possibly ‘splash’ or ‘droplet’ related), not necessarily positioned centrally to the “blue spot”. Corrosive-reaction product or sometimes pitting could be observed within the patches; Fig. 8(b).

Such patches were not optically visible adjacent to either the ST1 or ST2 “blue spots”, but as these components had been cleaned in preparation for prior non-destructive examination, they might have been removed. This is an aspect that made original “blue spot” diagnosis more difficult.

“Blue spot” fractography sometimes appears within more conventional hot LCF growth-out temper colouration. This was clear on specimen LCF133, where brittle “trans-lamellar cleavage” was seen optically to a depth of 0.23 mm, whilst blue to straw colouration was exhibited beyond the transition into conventional fatigue; Fig. 7(c). This is a potential cause for future confusion in identifying HSSCC against conventional fatigue growth-out cracking.

The non-salt-contaminated datum specimen (LCF127) showed only expected fatigue ‘growth-out’ temper colouration; brittle “trans-lamellar cleavage” characteristics were not observed.

3. Energy dispersive X-ray analysis (EDX)

SEM EDX was carried out on an Oxford Instruments INCA X-ACT system on the Leo 1550 FEG-SEM (in Rolls-Royce, Bristol), unless otherwise stated. Secondary electron images in Figs. 9–11 were taken on a Zeiss Auriga FEG-SEM at Imperial College.

EDX analysis on the side-face patches adjacent to the test specimen blue spots has revealed a chlorine presence [11].

Close examination of ST1 identified a tiny ‘surface-negative’ area (pit) of $12 \times 21 \mu\text{m}^2$ on the side-face immediately adjacent to the fracture surface blue spot; Fig. 9. Although no residue patch was observed, it is probable that the previous cleaning had removed it to expose a pit.

SEM-EDX analysis on the Zeiss Auriga FEG-SEM in Imperial College identified depleted titanium (Ti), and elevated oxygen (O), chlorine (Cl), sodium (Na) and trace calcium (Ca) within this surface negative area; Fig. 10 (X-ray dot maps) and Fig. 11 and Table 2 (semi-quantitative results).

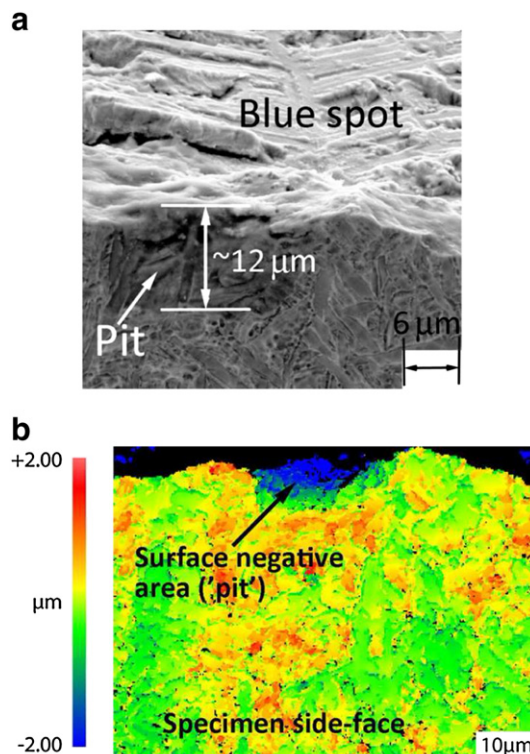


Fig. 9. (a) Secondary electron image of the ST1 specimen side-face surface (lower image half) with the blue spot on the fracture surface at high incline (upper image half). A surface negative area (pit) can be seen in darker contrast to the surrounding normal etched surface. (b) Imperial College false colour topographic image via light interferometry mapping of the ST1 specimen side-face showing surface negativity ($-2 \mu\text{m}$) of this area in blue.

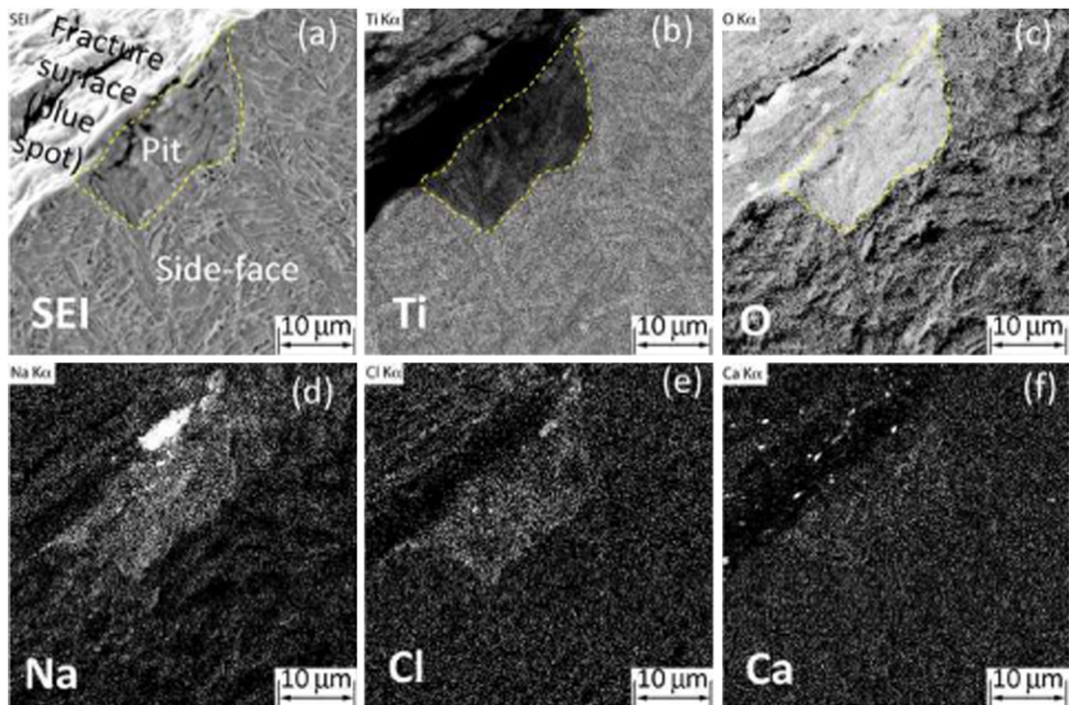


Fig. 10. EDX X-ray dot maps on specimen ST1 side-face pit. (a) Secondary electron image of the area mapped, with maps for (b) Ti K α (depleted), (c) O K α (elevated), (d) Na K α (elevated), (e) Cl K α (elevated), and (f) Ca K α (trace).

The above instigated a more focussed search for chlorine on the blue spot fracture surfaces. This included (i) overnight (16 h) X-ray mapping at low accelerating potentials (7.5 kV, 10 kV), and (ii) semi-quantitative line scans through and beyond the blue spot transition into fatigue.

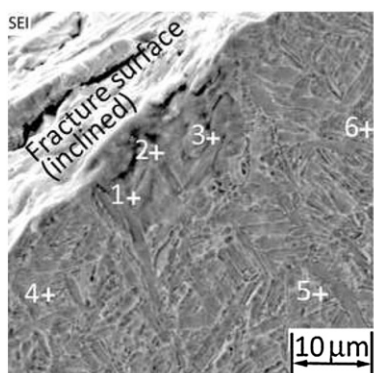
The long-duration EDX maps identified an oxygen presence, and faintly chlorine, that matched blue spot dimensions optically; Fig. 12, and in [11]. The more commonly-applied, shorter duration, higher potential EDX dot mapping did not reveal these elements.

The semi-quantitative line scan paths as carried out on specimen ST2 are depicted in Fig. 13.

Fig. 14 graphically depicts the results. A distinct change on either side of the blue spot periphery was identified for each element studied (despite scatter): A notable drop in O concentration, and a near-matching converse increase for Ti, whilst Na, Cl, K, Ca, and Mg existed in trace levels within the blue spot – dropping to zero or near-zero after transition.

The ST1 'blue spot' was analysed at Imperial, with very similar findings; Fig. 15.

Trace levels of Mg, Ca and K, in addition to Na and Cl, on the blue spot fracture surface suggested possible human contact in association with the original surface corrosive media. The 4 chief mineral elements in solutes derived from human perspiration are as in Table 3 [27].



	Composition – Atomic %							
	Ti	Al	Sn	Zr	Mo	O	Cl	Na
1	24	4.5	0.2	1.0	0.5	67	0.7	1.8
2	15	3.2	0.1	1.0	1.0	76	0.7	3.2
3	24	4.9	0.3	0.9	0.4	67	0.9	1.7
4	41	5.7	0.4	1.5	0.3	50	-	0.9
5	44	4.7	0.5	1.9	2.2	46	-	0.6
6	45	7.0	0.5	1.5	0.4	45	-	0.5

Fig. 11 and Table 2. Semi-quantitative EDX spot analyses within and outside the ST1 pit. Enrichment of O and depletion of Ti with low levels of sodium and chlorine confirmed (with some Na outside the pit at a lower level).

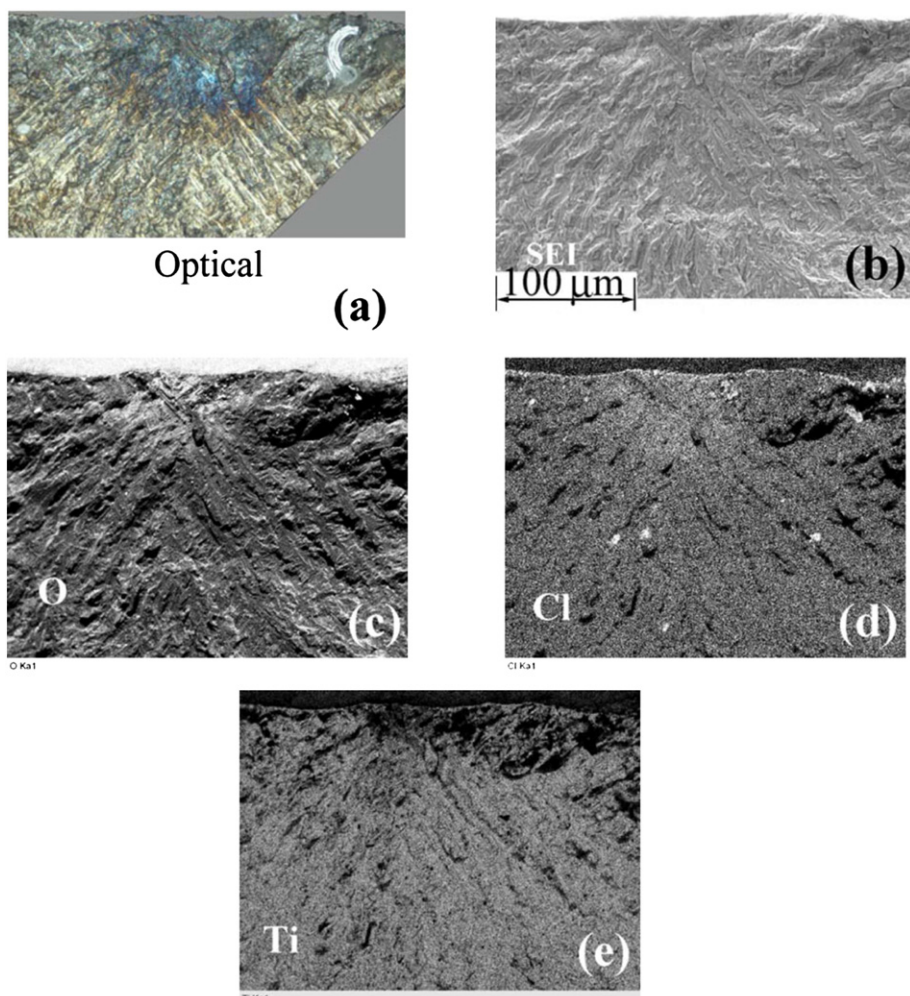


Fig. 12. (a) and (b) Blue spot fractographs compared against low potential long term duration SEM-EDX dot maps for ST2: (c) Ti K α , (d) O K α and (e) Cl K α . Although faint, the oxygen 'marks out' the blue spot shape, with tentative Cl visual evidence.

As no corrosive media side-face 'patches' were found either on ST1 or ST2, barring the tiny surface pit on ST1, it is plausible that such had been cleaned off or been difficult to see prior to cleaning – circumstantially, this further suggests possible original human fingerprint contamination.

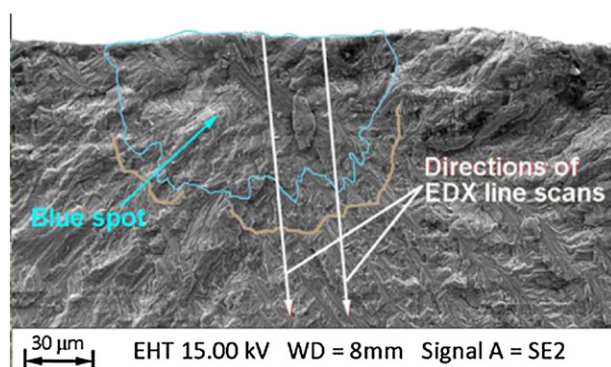


Fig. 13. Depiction of the semi-quantitative EDX line scan directions across the specimen ST2 'blue spot'. The blue line depicts the optically blue periphery, and the brown line the periphery of a surrounding narrow dark straw-coloured band. Compare with optical image; Fig. 7b.

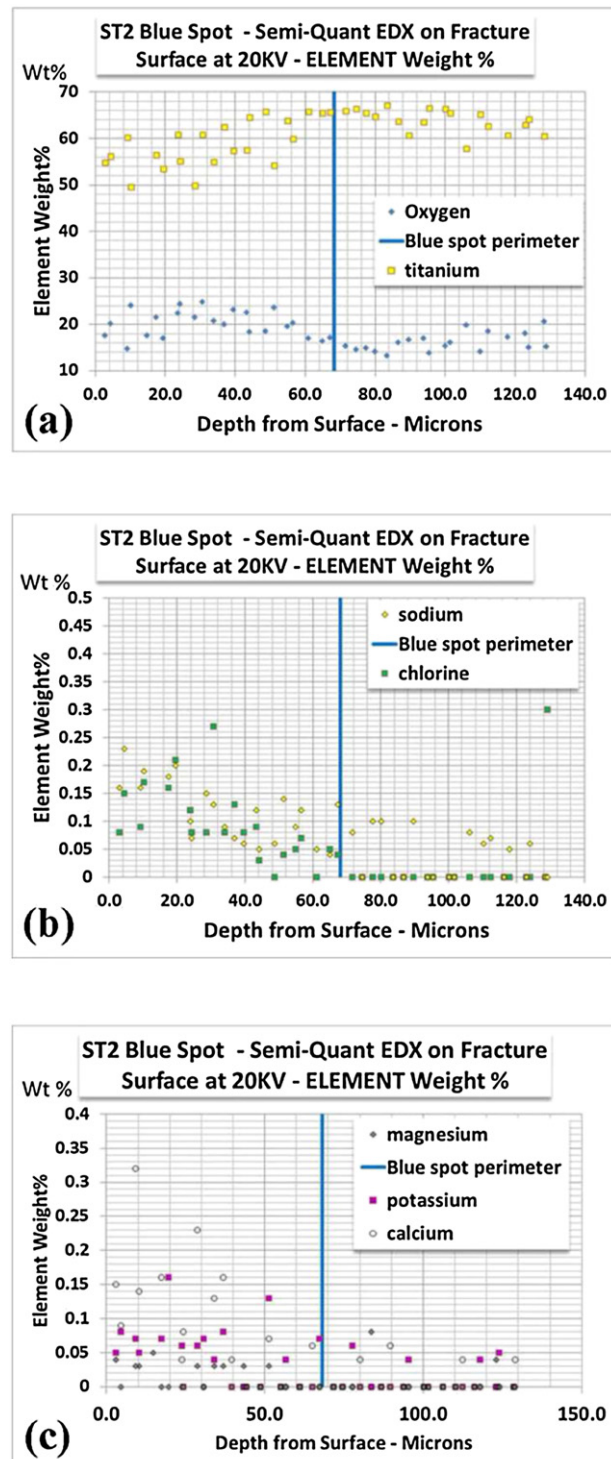


Fig. 14. 20 kV EDX semi-quantitative analysis line scans through the ST2 blue spot – in weight %. Percentages given are based on numbers of X-rays emitted from the electron beam penetration volume (not a precise interpretation of surface layer composition). Either side of the blue spot periphery, (a) O drops from 15–25% to 12–20%, Ti from 50–60% to 60–70%, (b) Cl and Na drop ‘dramatically’ from 0.05–0.25% to near 0%, and (c) trace K, Ca and Mg drop to near 0%.

Similar analyses were performed on the known salt-contaminated LCF test specimen LCF133, with similar findings; Fig. 16. Mg, Ca and K were not identified in semi-quantitative EDX analysis of the blue spot fracture surface, for in that case NaCl had been applied in a purer form (not human perspiration derived).

A full repeat EDX study of the non-salt-contaminated datum specimen (LCF127) origin did not find evidence of Na, Cl, Mg, Ca or K.

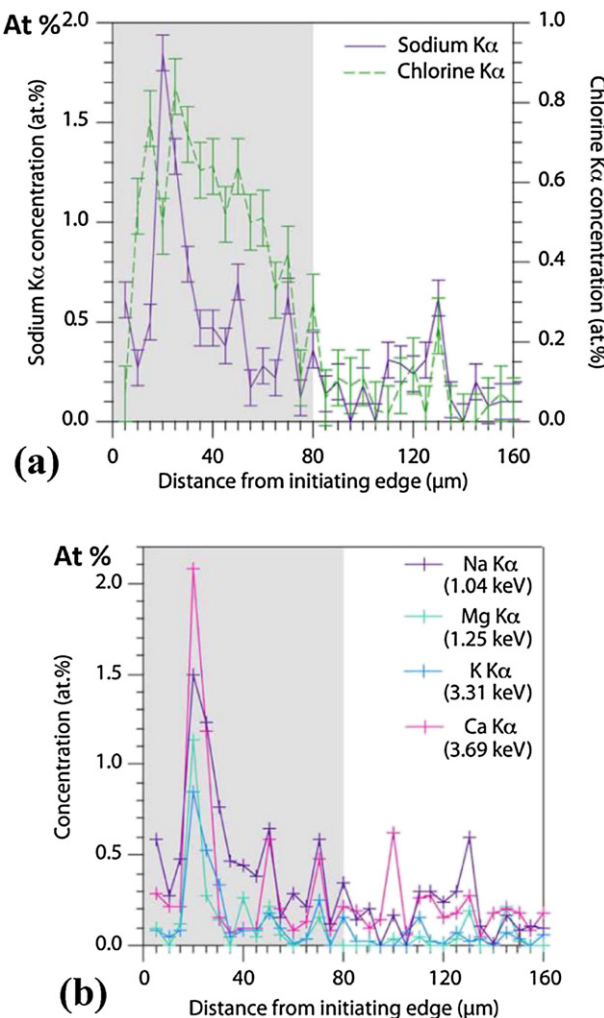


Fig. 15. 20 kV semi-quantitative EDX line scans through the ST1 ‘blue spot’ (marked in grey) in atomic %, for (a) Na and Cl, (b) Na, Mg, K and Ca, all existing at low levels in the blue spot, dropping to near-zero after its periphery.

4. Focussed ion-beam with secondary ion mass spectrometry (FIB-SIMS) of the specimen side-face patches

FIB-SIMS dynamic depth profiling experiments were performed using a FEI FIB200-SIMS microscope at Imperial College as shown in Fig. 17 and as described in [11].

The methodology used for interpretation of the side-face patches adjacent to the fracture surface blue spots is described in [11], although brief salient features are re-produced here:

Ions were sputtered from the sample surface by bombardment with gallium ions (with 30 keV energy) from a liquid metal source. Innovatively, the system was operated such that positive and negative sputtered ions could be detected simultaneously – the former by a FEI FIB200-SIMS detector, the latter by a Hiden EQS1000 system [11,28].

Table 3
Average levels of the 4 chief elements identified
in human perspiration [27].

Element	g/l
Na	0.9
K	0.2
Ca	0.015
Mg	0.013

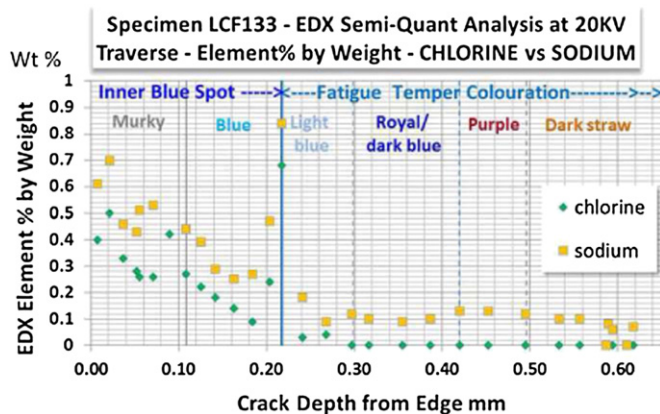


Fig. 16. Graphical display of 20 kV semi-quantitative EDX line scans through a LCF133-specimen blue spot fracture surface – for Na and Cl only: Both were detected to percent fractions within the blue spot, but dropped to near-zero beyond.

All sites subject to FIB-SIMS compositional analysis were pre-sputter cleaned using the FIB-SIMS primary gallium ion beam at a current of 20 nA (Fig. 17a). This cleans up the upper layers, so that initial data coming from the trenches can be judged uninfluenced by contamination. A series of trenches (depth profile craters), each of dimension $2 \times 50 \mu\text{m}$ (depth at least 1 μm), were then FIB-milled with a 3 nA gallium ion beam. The trenches were closely spaced (2 μm) through the side-face patches (initial 40 μm depth), then with increasing separation (10 μm) beyond; Fig. 17b.

A second set of trenches were milled >1 mm from the original set, to allow datum result-comparison. Bulk mass spectrum analysis and baseline data were also obtained remote from the blue spot area [11]. The experimental methodology, including reason for the trench dimension selection, is described in detail in [11].

For ST1, LCF133 and other specimens [11], elevated $^{16}\text{O}^-$, $^{35}\text{Cl}^-$, and $^{23}\text{Na}^+$ ions were identified in the profiles close to the fracture surface within the side-face patches (Fig. 18), although not found for specimen ST2. The same procedure on the control specimen LCF127 did not identify any significantly elevated $^{35}\text{Cl}^-$ or $^{23}\text{Na}^+$ compared to the datum trenches.

5. Energy dispersive X-ray analysis by scanning transmission electron microscopy (STEM-EDX) on fracture surface FIB “lift-outs”

TEM foils were produced from the blue spot fractures of samples ST1, ST2, LCF133 and LCF127 (datum) using a focussed ion beam (FIB) lift-out technique at Imperial College using a dual beam FEI Helios NanoLab 600 with the primary Ga^+ beam. The method is shown in Fig. 19, and described more fully in [11]. Foils were extracted from the ‘blue spot’ fracture surface, with results compared against foils lifted from the remote fatigue surface [31,32].

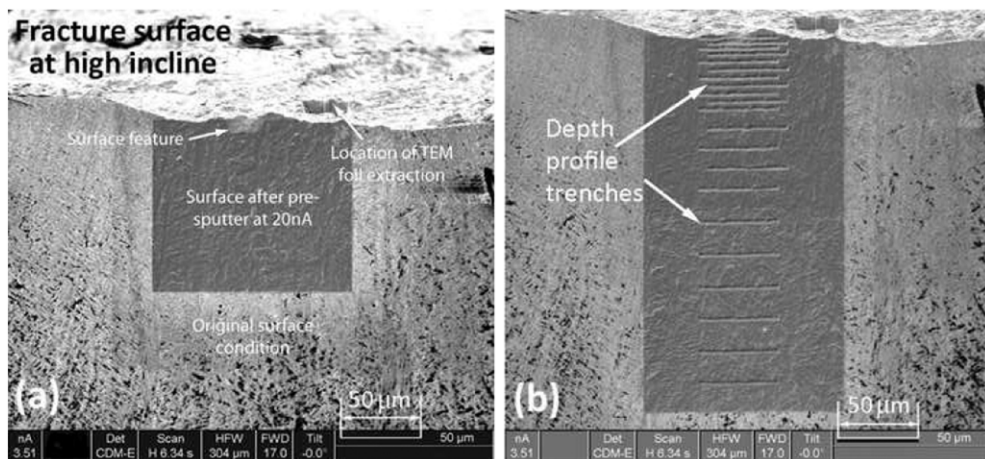


Fig. 17. FIB-SIMS dynamic depth profiling for chemistry-interpretation, applied here to the specimen ST1 side-face surface feature (patch) adjacent to the fracture surface blue spot. (a) Shows the pre-sputter cleaned area. (b) Shows the trenches (depth profile craters). The location of the TEM ‘lift-out’ foil (as described in Section 5) on the fracture surface can be seen in both images.

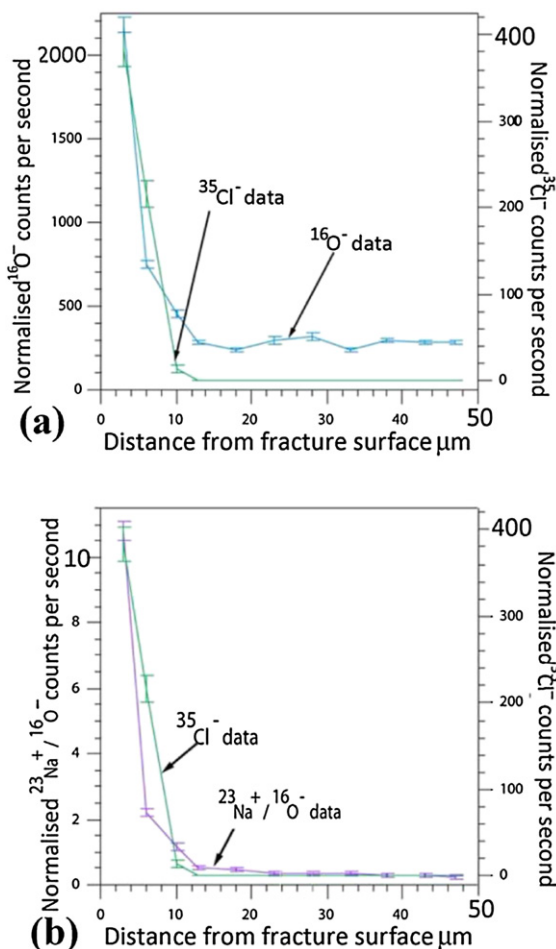


Fig. 18. Sputtered secondary ion profile FIB-SIMS data from specimen ST1 plotted against distance from the 'blue spot' fracture surface (in μm), with each measurement point taken from the base of individual trenches. The profiles are: (a) $^{16}\text{O}^-$ and $^{35}\text{Cl}^-$, (b) $^{23}\text{Na}^+ / ^{16}\text{O}^-$ and $^{35}\text{Cl}^-$, with elevation for each over the initial 10 μm from the fracture surface. Ambient oxygen can enhance positive secondary ion yield [11,29,30], so the $^{23}\text{Na}^+ / ^{16}\text{O}^-$ ratio has been used to account for increased oxygen content in the initial 10 μm from the fracture surface — elevated $^{23}\text{Na}^+$ remains apparent.

The foils were then subject to STEM-EDX, focussing on the surface layer beneath the protective platinum layer — via mapping and semi-quantitative line scans. In [11] the surface layer was shown as an oxide film with an approximate 1:2 Ti:O atomic ratio (suggesting TiO_2), also containing chlorine less than 1% atomic weight.

The EDX maps demonstrated the oxide film to have variant thickness but typically ~200 nm (Fig. 20), occasionally dropping to ~50–100 nm. Chlorine was partly intermingled and lying immediately beneath the oxide layer (Fig. 20), suggesting the Cl presence to be a result of a reaction process, not post-contamination. Line scans through the oxide into the parent microstructure confirmed elevated O, Cl, with traces of Ca, K and Mg (Fig. 20).

Fig. 20(d) and (e) shows the elements O, Cl, Na, Mg, K and Ca present and confined to the oxide layer within the ST1 blue spot; Na and Cl rose to 1.3–1.4% with an additional peak toward the oxide layer base, dropping to ~0% in the parent material.

Similar findings were established on foils extracted from ST2 and LCF133. Furthermore, foils lifted from (1) fatigue remote from the blue spots, and (2) the fatigue origin of specimen LCF127 (datum), did not show evidence of elevated Cl, and had much lower oxide thickness (~20 nm).

It is not the intention of this article to discuss the reason for the blue colour, though it is postulated that it may relate to the mix of Cl within the oxide layer, in addition to thin film interference effects.

6. Discussion – mechanism and chemistry

The proposed reaction chemistry behind the HSSCC_{NaCl} mechanism is described within [11], as largely derived from interrogation of previous research [2,6,11,33–39]. It is considered that the HSSCC mechanism generates a level of hydrogen-embrittlement [6,11,33,34,37–39]. Very low levels of Ca, K (and trace Mg) in addition to Na/Cl, combined with observational difficulty of corroded

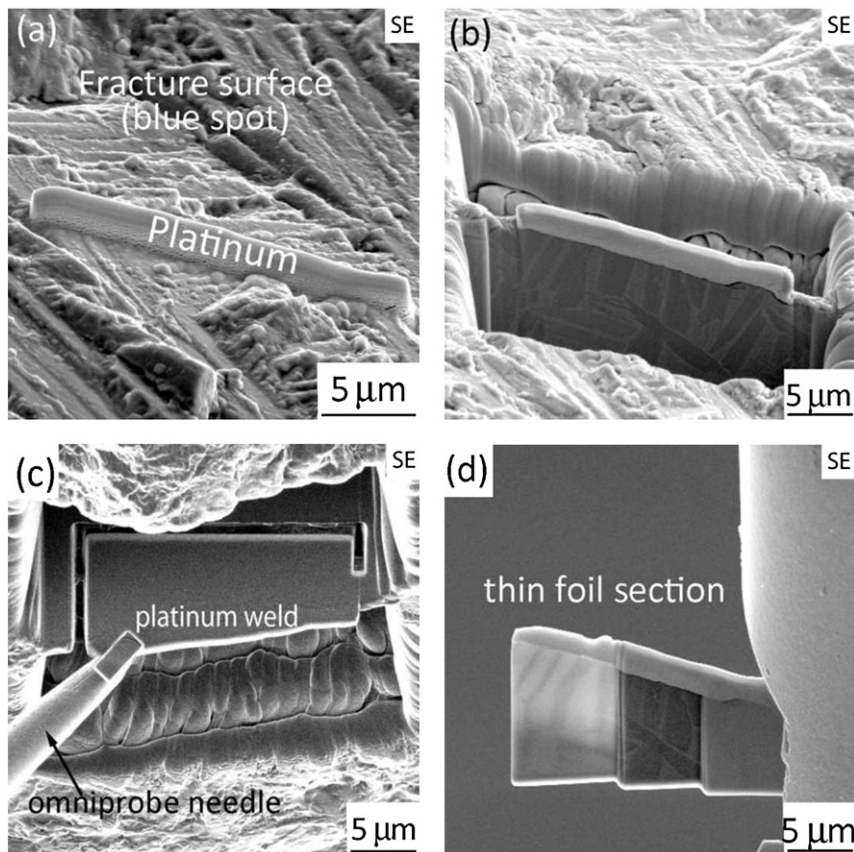


Fig. 19. Producing a "lift-out" foil from the blue spot fracture surface: (a) A platinum-containing layer is initially deposited with the FEI Helios NanoLab 600 gas injection system – this protects the area of interest underneath from the FIB beam. (b) Material is FIB-milled around the protected area to a depth of several microns. (c) An omniprobe needle is platinum-welded to the potential foil following FIB milling around the periphery bar a small ligament – which is then cut to allow foil removal. (d) The foil is welded to a TEM omniprobe grid, and then further thinned by FIB milling to allow electron passage (three stages of thinning may be seen – with microstructure visible in the thinnest area, ~150 nm).

patches on specimens ST1 and ST2, suggest human contact (perspiration, fingerprints) might have initially caused contamination with ultimate fatigue initiation-life reduction.

For the purpose of this article, a much-shortened version of the chemistry explanation follows:

At temperatures $> -550^{\circ}\text{F}$ ($\sim 290^{\circ}\text{C}$) for similar disc alloys to Ti6246 [1,2,34,40], a patch of salt (NaCl) can react with the protective surface oxide to form sodium titanates (e.g., Na_2TiO_3) and hydrochloric acid (HCl) [11,35,39,41]. On breaking this passive layer, un-oxidised titanium beneath the patch may react with the HCl , producing titanium-alloy chlorides and atomic hydrogen that can 'charge' the parent [2,11,34,35,39,42]. Thermodynamic analyses indicate that HCl preferentially attacks aluminium and tin in the alloy [39,43,44], generating more hydrogen than from attack of the titanium alone [39].

Ti-alloy chlorides then react with moisture (H_2O) to produce Ti , Al and Sn oxides over the reaction site, and further HCl [33,34,39]. This is a looping pyrohydrolysis reaction where HCl generated can continue to react with exposed titanium, producing more hydrogen [11,39].

In this situation, the balance of hydrogen-charging versus the diffusion into the bulk material (dilution) favours charging and the material becomes locally embrittled. If applied tensile stress overcomes the resulting reduced fracture toughness, then cracking takes place [2,11,33]. This is the initiation of the hot salt stress corrosion crack.

Continuation of the looping reaction embrittles the crack tip with further hydrogen, and cracking advances as long as the applied stress-intensity exceeds locally reduced fracture toughness at the crack tip [11,33], leaving a brittle fractographic appearance [2,11,24–26,33,34] and a layering of corrosion by-products away from the reaction surfaces (titanium-alloy chlorides, sodium titanate, then oxides such as TiO_2) [11,34,35,39]. It follows that if the pyrohydrolysis reactions are going to produce HSSCC then it should occur early in a test when the reactions are likely to be at their most vigorous, or not all, consistent with striation evidence and Fracture Mechanics analysis.

In a simple experiment to assess thermodynamic favourability of these reactions, Ti-230 alloy plates were immersed overnight in a mixture of NaCl and TiO_2 at temperatures of 450°C and 500°C . On removal, a yellow-tinged deposit at localised sites indicated reaction (Fig. 21), similar to that seen in [35]. Although Na_2TiO_3 was not directly identified in the deposit by EDX analysis, it consisted of a mix of Ti , O , Na , Cl and other alloy elements (Cu , Fe). Of particular note is that subsequently scraping off the sample deposit areas

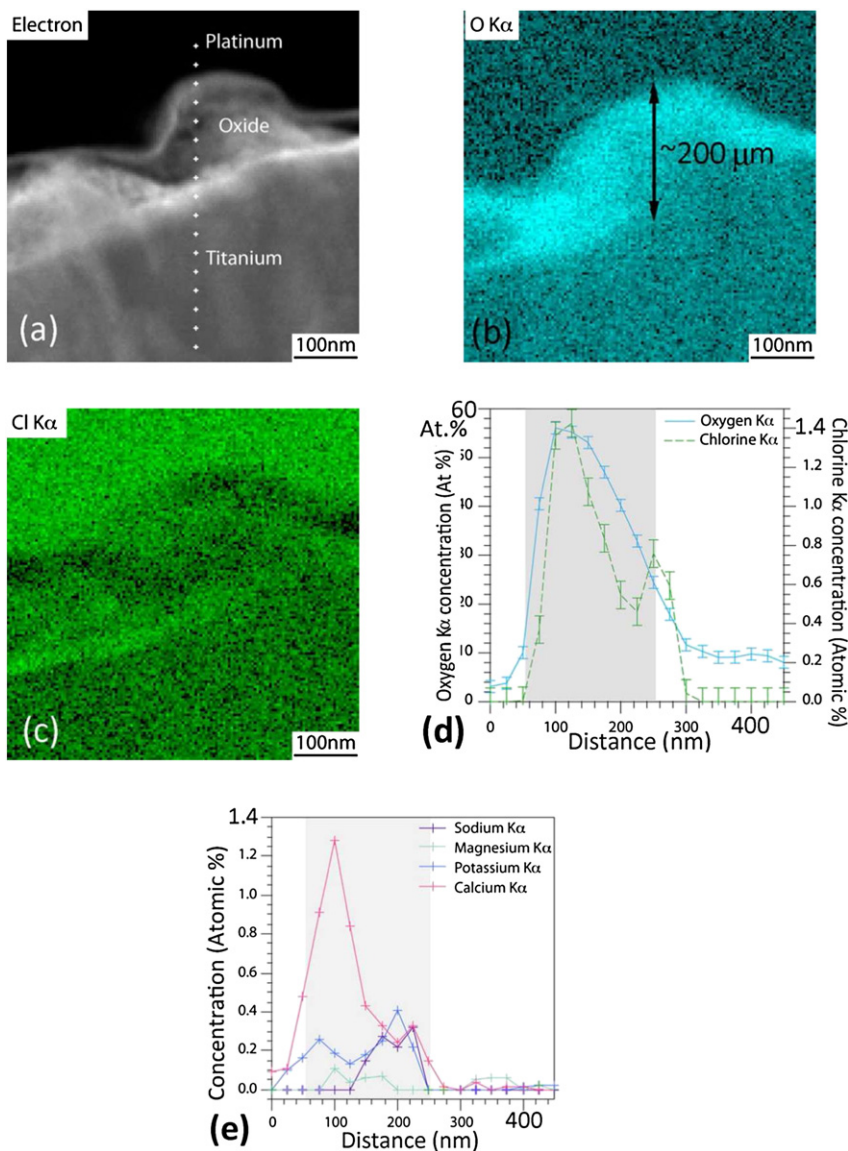


Fig. 20. (a) TEM electron image of an example area from a specimen ST1 blue spot fracture surface ‘lift-out’ foil – with ~200 nm oxide film. The spots indicate the semi-quantitative EDX line scan path. (b) O K α EDX map displaying the oxide layer. (c) Cl K α EDX map showing ‘intermingling’ of low level Cl through and underneath the oxide layer. The Pt layer is also visible (green) because there is a Pt M_{III} line of similar excitation energy (2.65 keV) and intensity to the Cl K α peak (2.62 keV) [11]. Semi-quantitative line scan results in atomic % are shown for (d) O and Cl, and (e) Na, Mg, K and Ca. The grey area indicates the oxide film.

initiated a reaction with airborne moisture consisting of gaseous bubbling and a black deposit, as per [40] (EDX: richer in Cl), with subsequent pit formation (Fig. 21). The level of reaction was more vigorous following 500 °C exposure than at 450 °C.

HSSCC cracks usually have a finite area, indicating exhaustion of original corrodant supply and of the consequent reaction hemistry with H-production tailing off. A potential explanation is as follows: At 450 °C, there are five Ti6246-alloy chlorides [11,39,45], which react with water to form oxides over the reaction site. Three of these chlorides are vapour and can progressively escape, especially as the corrosion crack growth exceeds the reaction site that initiated it: Combined with an increasing crack area (dilution), this reduces HCl concentration, reaction rate and consequential H-charging at any given point on the crack tip. Local fracture toughness in the embrittled zone rises and, when it exceeds the stress intensity at the HSSCC crack tip, the mechanism halts. Transition to LCF then occurs if the crack tip stress-intensity amplitude ΔK is large enough for fatigue to progress. This is thought to explain the often-observed abrupt transition from HSSCC to LCF (eg. Fig. 5).

There is an alternate hot reaction – that of Ti-alloy chlorides with oxygen (O_2) to form Ti-alloy oxides, predominantly TiO_2 , and Cl_2 – neither HCl nor hydrogen [11,39]. At typically elevated engine operation pressures (higher oxygen partial pressures), that reaction is favoured over the pyrohydrolysis one such that HCl-formation diminishes. Consequently, the balance of hydrogen-charging versus

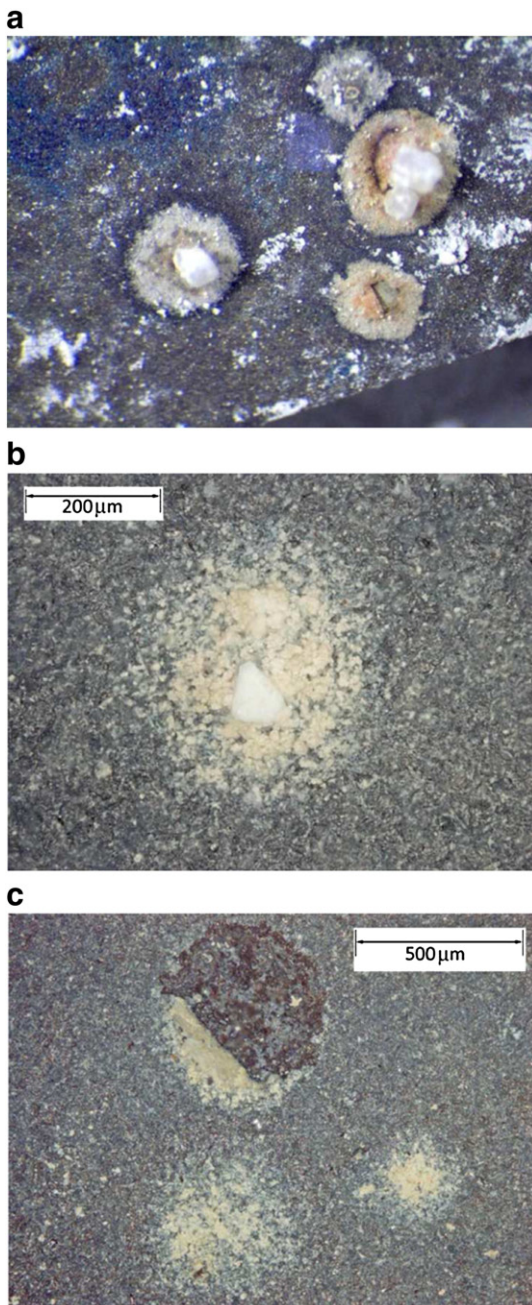


Fig. 21. Optical images of yellow-tinged reaction product on Ti-230 alloy plate by NaCl following overnight exposure at 450 °C – beneath individual NaCl crystals ((a) and (b)). (c) Also shows a darkened pit in the upper half of the image that formed where the reaction product came away – this was richer in Cl (with very little Na) than the yellow material. Compare ref 35 Fig. 1.

diffusion away favours the latter, and the material does not attain a sufficient level of embrittlement to crack under prevailing tensile stress and HSSCC does not occur.

The above is supported by Cranfield University data from 1994 [39], which showed notable improvements in the life of salt-coated Laboratory LCF specimens with increasing pressure [39], depending on applied stress; eg. Fig. 22.

A hydrolysis reaction of remnant Ti-alloy chlorides, from the high temperature reactions, can also occur at room temperature [35,41], but the H-charging rate is likely to be relatively slow [35]. Although diffusion away from the local concentration is also likely to be slower, the material does not achieve a sufficient level of embrittlement to lead to cracking when next loaded, and the stress-corrosion cracking process is suppressed.

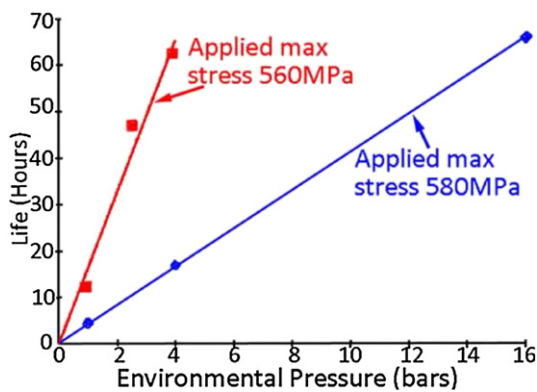


Fig. 22. Demonstrating significant improvements in life with pressure for salt-coated LCF specimens (on alloy IMI834 at 500 °C) – from work at Cranfield University in 1994 [39]. Two lines for two different applied stress conditions (560 and 580 MPa) are shown.

The above explains why HSSCC_{NaCl} is not observed in engine service, but is confined to Laboratory specimen and component spin rig tests at atmospheric pressure and below [1].

7. Conclusions

Small (~0.1 mm across) optically blue or blue/grey features (“blue spots”) at LCF origins of two Ti-6246 alloy hot cyclic fatigue spin tests, not formerly explained, have now been understood via the collaboration of Rolls-Royce (Industry) with Imperial College (Academia) by combining elements of classical failure analysis with developed existing and novel technologies. Repeatability, despite some variability, of results from “blue spot” LCF laboratory test specimens and negativity in datum (non-contaminated) samples, has lent confidence to the following conclusions:

1. The “blue spots” were due to a hot salt stress-corrosion cracking mechanism that stemmed from small surface sodium chloride (NaCl) contaminant deposits – HSSCC_{NaCl}. Transition to conventional low cycle fatigue (LCF) occurred at ~0.1 mm depth, relating to exhaustion of the original contaminant reaction chemistry.
2. Propagation from the “blue spot” had occurred with a near-nil initiation life, as demonstrated by validated striation counting combined with fracture mechanics logic.
3. Advocated by focussed EDX work, STEM-EDX measurements on TEM foils FIB lifted from blue spot fracture surfaces found a relatively thick ~200 nm TiO₂ surface layer, with trace Cl mixed within and underneath the layer (confirming a process of corrosive-reaction chemistry, not post-contamination).
4. Evidence supported probable original contamination by ‘human touch’ (eg fingerprint).
5. Previous research interrogation shows hot reaction chemistry of NaCl with titanium alloys that generates hydrogen as a consequence of a looping pyrohydrolysis reaction at high temperature and “low” pressure. Fracture toughness is locally reduced by hydrogen-charging, and if sufficiently low, cracking occurs under applied tensile stress – resulting in brittle trans-lamellar cleavage fractography (HSSCC).
6. The proposed lack of implication for the HSSCC_{NaCl} mechanism in operation under the high pressures of the gas turbine environment is based on an alternate hot reaction chemistry with O₂ occurring at increased oxygen partial-pressure that do not generate hydrogen (competing with the pyrohydrolysis reaction). In this way the hydrogen charging rate slows, insufficient to allow HSSCC.

Acknowledgements

The authors would like to thank members of the Rolls-Royce Deutschland Failure Analysis team (Dahlewitz, Germany) for their work on the ST1 and ST2 investigations, provision of test specimens, and support – Karin Frank, Heike Floege, Matthias Goebel, Sarah Mouti, and Gunter Friedel.

We would also like to thank John Chamberlain, Jane Woolrich, Mark Dixon and Alex Davidson of Rolls-Royce plc; the former for his work on the reaction chemistry understanding, and the latter three for their support and test specimen provision.

The images and graphs shown in Figs. 9–11, 15, and 17–20 were provided by Tamara Chapman.

References

- [1] R.W. Schutz, D.E. Thomas, Corrosion of titanium and titanium alloys, ASM International HandbookCorrosion, vol. 131998, 669–706 (sixth printing).
- [2] R.W. Schutz, Stress-corrosion cracking of titanium alloys, Stress-Corrosion Cracking: Materials Performance and Evaluation, ASM International, 1992, 265–294.
- [3] G. Lütjering, J.C. Williams, Titanium, Second ed. Springer, New York, 2003.
- [4] H. Ghonem, Microstructure and fatigue crack growth mechanisms in high temperature titanium alloys, Int. J. Fatigue 32 (2010) 1448–1460.
- [5] M. Whittaker, Titanium in the Gas Turbine Engine. Advances in Gas Turbine Technology. InTech, edited by E Benini. Chapter 14, p 315–336
- [6] I. Chatteraj. Stress corrosion cracking (SCC) and hydrogen-assisted cracking in titanium alloys. Stress Corrosion Cracking: Theory and Practice – chapter 10, p 381–408. Woodhead Publishing - Edited by V.S. Raja, T. Shoji.

- [7] D. Eylon, S. Fujishiro, P.J. Postans, F.H. Froes, High-temperature titanium alloys – a review, *JOM* 1 (6) (Nov. 1984) 55–62.
- [8] Ti-6Al-2Sn-4Zr-6Mo. Materials Properties Handbook: Titanium Alloys, p 465–481 – ASM International. Edited by G. Welsch, R. Boyer, E. W. Collings
- [9] J. Mendez, On the effects of temperature and environment on fatigue damage processes in Ti alloys and in stainless steel, *Mater. Sci. Eng. A* 263 (2) (May 15 1999) 187–192.
- [10] G. Asquith, A.C. Pickard, Fatigue testing of gas turbine components, in: K.J. Marsh (Ed.), Chapter 11 of Full-Scale Fatigue Testing of Components and Structures, Butterworths, 1988.
- [11] T.P. Chapman, R.J. Chater, E.A. Saunders, A.M. Walker, T.C. Lindley, D. Dye, Environmentally assisted fatigue crack nucleation in Ti-6Al-2Sn-4Zr-6Mo, *Corros. Sci.* 96 (2015) 87–101.
- [12] D. Benoit, R. Namdar-Irani, R. Tixier, Oxidation of fatigue fracture surfaces at low crack growth rates, *Mater. Sci. Eng.* 45 (1) (August 1980) 1–7.
- [13] G.F. Vandar Voort, Visual Examination and Light Microscopy. ASM Handbook Vol 12 "Fractography". ASM International.
- [14] T.L. Anderson, Fracture Mechanics: Fundamentals and Applications, Second ed. CRC Press LLC, 1995.
- [15] A.L. Pilchak, A. Bhattacharjee, A.H. Rosenberger, J.C. Williams, Low ΔK faceted growth in titanium alloys, *Int. J. Fatigue* 31 (2009) 989–994.
- [16] S.H. Wang, C. Müller, A study on the change of fatigue fracture mode in two titanium alloys, *Fatigue Fract. Eng. Mater. Struct.* 21 (1998) 1077–1087.
- [17] D.J. Wulpi, Understanding how Components Fail, in: B. Miller (Ed.) 3rd ed. ASM International, 2013 (Chapter 10 – Fatigue Fracture, reviewed and revised by N.E. Cherolis and W.D. Pridemore).
- [18] P.H. DeVries, K.T. Ruth, D.P. Dennies, Counting on fatigue: striations and their measure, *Microsc. Microanal.* 15 (Supplement S2) (July 2009) 500–501.
- [19] N.E. Cherolis, Fatigue in the aerospace industry: striations, *J. Fail. Anal. Prev.* 8 (2008) 255–258.
- [20] W.C. Connors, Fatigue striation spacing analysis, *Mater. Charact.* 33 (3) (October 1994) 245–253.
- [21] L.R. Botvina, L.V. Limar, Relationship of the spacing of the fatigue striations to the range in the stress intensity factor, Soviet Mater. Sci.:Transl. Fiziko-khimicheskaya Mekhanika Materialov/Acad. Sci. Ukrainian SSR 21 (2) (March–April, 1985) 144–152.
- [22] Ministry of Defence, Defence Standard 00-970 Part 11, Issue 5, Jan 2014.
- [23] E.E. Gdoutos, Fracture Mechanics: An Introduction, Second ed. Springer, 2005.
- [24] J.C. Williams, Some observations on the stress-corrosion cracking of three commercial titanium alloys, Boeing Company D6-19553Sept 1967. (Sponsored by Advanced Research Projects Agency ARPA Order No. 878).
- [25] R.E. Curtis, Relationship between composition, microstructure, and stress-corrosion cracking in titanium alloys, Boeing Company D6-23716Oct 1968. (Sponsored by Advanced Research Projects Agency ARPA Order No. 878).
- [26] R.L. Fowler, A.J. Luzietti, Hot Salt Stress Corrosion Studies, United Technologies Corporation Pratt and Whitney Aircraft Group, USA, June 1st 1978.
- [27] S.J. Montain, S.N. Cheuvront, H.C. Lukaski, Sweat mineral-element responses during 7 h of exercise-heat stress, *Int. J. Sport Nutr. Exerc. Metab.* 17 (6) (2007) 574–582.
- [28] R.J. Chater, B.A. Shollock, D.S. McPhail, A.J. Smith, G. Cooke, Differentially pumped quadrupole SIMS probe on FIB-based and two-beam microscopes, *Surf. Interface Anal.* (2014), <http://dx.doi.org/10.1002/sia.5665> (in press,available online).
- [29] J. Kikuma, H. Imai, Yield enhancement effect of low-energy O_2^+ ion bombardment in Ga focused ion beam SIMS, *Surf. Interface Anal.* 31 (2001) 901–904.
- [30] T. Sakamoto, B. Tomiyasu, M. Owari, Y. Nihei, Ambient oxygen effect in Ga⁺ FIB-SIMS, *Surf. Interface Anal.* 22 (1994) 106–110.
- [31] W.M. Phaneuf, Applications of focussed ion beam microscopy to materials science specimens, *Micron* 30 (1999) 277–288.
- [32] L.A. Giannuzzi, B.W. Kemphall, S.M. Schwarz, J.K. Lonness, B.I. Prentizer, F.A. Stevie, FIB lift-out specimen preparation techniques, in: L.A. Giannuzzi, F.A. Stevie (Eds.), From 'Introduction to Focussed Ion Beams: Instrumentation, Theory, Techniques, and Practise', Springer, New York 2005, pp. 201–228.
- [33] J.R. Myers, J.A. Hall, Hot salt stress-corrosion cracking of titanium alloys: an improved model for the mechanism, *Corros. – NACE* 33 (7) (1977) 252–257.
- [34] S.P. Rideout, M.R. Louthan Jr., C.L. Selby, Basic mechanisms of stress-corrosion cracking of titanium, *Stress-Corrosion Cracking of Titanium*, ASTM STP 397, Am. Soc. Testing Mats, 1966. 137–151.
- [35] V.C. Petersen, H.B. Bomberger, The mechanism of salt attack on titanium alloys, *Stress Corrosion Cracking of Titanium: ASTM Special Technical Publication*, 3971966. 80–94.
- [36] G. Lapasset, Study of hot stress corrosion cracking of TA6V (Ti-64) alloy by sodium chloride, *Rech. Aerospaciale* Issue 191 (July 1979) 255–261.
- [37] J.B. Cotton, Stress-corrosion of titanium alloys, AGARD Conference Proceedings Series No. 18 – Stress Corrosion Cracking in Aircraft Structural Materials, Research Dept Imperial Metal Industries Ltd, Witton, Birmingham, April 1967.
- [38] X. Demulants, J. Mendez, Influence of environment on low cycle fatigue damage in Ti6Al4V and Ti 6246 titanium alloys, *Mater. Sci. Eng. A* 219 (1–2) (November 30 1996) 202–211.
- [39] T.C. Chevrot, J.R. Nicholls, Pressure Effects on the Hot-Salt Stress-Corrosion Cracking of Titanium Alloys(Thesis/Dissertation) School of Industrial and Manufacturing Science – Cranfield CERES University, March 1994.
- [40] N.G. Fiege, L.C. Covington, Overview of corrosion cracking of titanium alloys, *Stress-Corrosion Cracking of Metals – A State of the Art* by H. Lee Craig, ASTM Second Printing, April 1983. 119–130.
- [41] V.C. Petersen, Hot-salt stress-corrosion of titanium: a review of the problem and methods for improving the resistance of titanium, *JOM* (1971) 40–47.
- [42] M. Garfinkle, An electrochemical model for hot-salt stress-corrosion of titanium alloys, *Metall. Trans.* 4 (7) (July 1973) 1677–1686.
- [43] M.J. Blackburn, J.C. Williams, Metallurgical aspects of the stress corrosion of titanium alloys, *Proceedings of Conference on Fundamental Aspects of Stress-Corrosion Cracking*, 1969.
- [44] S.P. Rideout, R.S. Ondrejcin, M.R. Louthan Jr., Hot-salt stress corrosion cracking of titanium alloys, in: R.I. Jaffee, N.E. Promisel (Eds.), From The science, technology and application of titanium, Pergamon Press 1970, pp. 307–320.
- [45] R.S. Ondrejcin, M.R. Louthan Jr., Role of hydrogen chloride in hot-salt stress corrosion cracking of titanium-aluminium alloys, NASA CR-11331968.